Applied Mathematical Sciences, Vol. 15, 2021, no. 8, 357 - 368
HIKARI Ltd, www.m-hikari.com
https://doi.org/10.12988/ams.2021.914515

Temperature Distribution for Magnetohydrodynamic Flow in Straight Horizontal Elliptical Pipe

David Kweyu, A. Wanyama Manyonge

Department of Pure and Applied Mathematics
Maseno University, Kenya

K. Jacob Bitok

Department of Mathematics and Computer Science
University of Eldoret, Kenya

Abstract

A study has been carried out on temperature distribution on Magnetohydrodynamic (MHD) fluid flow in a pipe of elliptical cross section. Fluid is electrically conducting, viscous and incompressible. Governing equations are partial differential equations comprising Ohm's Law of electromagnetism, heat energy equation, equation of continuity and cross section of the pipe. Heat energy equation is converted into ordinary differential equation embracing similarity transformation and solved by Finite Element Method. Findings are in form of tables and contours and affirm that: Peak temperature of the fluid decreases at the centre of the pipe when Prandtl number is increased but increases on raising Hartmann number and Eckert number. In all the three situations, temperature diminishes towards the boundary of the pipe.

Mathematics Subject Classification: 35Q05

Keywords: Stream Function, Discretization, Elliptical Cross Section

1 Introduction

Temperature distribution characteristics of Magnetohydrodynamic (MHD) flows in pipes has many practical applications such as in electronic components, high temperature plasmas, chemical processing equipment, cooling of nuclear reactors, MHD accelerators etc [3]. Gedik *et.al* [8] studied the steady, laminar, incompressible viscous flow of an electrically conducting fluid in a circular non-conducting pipe numerically. They found that velocity decreased with an increase in the intensity of applied magnetic field. Abdulhassan *et.al* [1] numerically studied heat transfer of a fully developed turbulent flow inside elliptical tube with different aspect ratio of constant surface area. Multi-phase mixture model was used to calculate the Nusselt number, nanofluid velocity, and pressure drop. The three-dimensional Navier-Stokes, energy, and volume fraction equations were solved by ANSYS fluent with Finite Volume Method (FVM). Results showed that increase in nanoparticles concentration increases the Nusselt number with little pressure drop rise. The elliptical tube with 0.25 aspect ratio gives best enhancement in heat transfer compared with circular tube with maximum Nusselt number (52.9%).

2 Formulation of the problem

We investigate a case where a steady, viscous, incompressible and electrically conducting fluid flow in a straight long horizontal conducting pipe of elliptical cross section in the x-y plane as shown in figure 1, Kweyu *et.al* [7]. The fluid flows through the pipe due to Lorentz force and gravitational force. An applied magnetic field with an intensity $\mathbf{B}$ is parallel to the y-direction. The domain, Ω, is the elliptical cross section of the pipe and the boundary, Γ, is the inside of the cross section of the pipe.

2.1 Assumptions

i The flow is steady and there is no viscous dissipation of energy i.e $q = 0$

ii. Directed magnetic field is incident on the pipe parallel to the y-axis and perpendicular to the z-axis. It varies in the direction r and θ but is zero in z direction, the magnetic field is : $\mathbf{B} = \{B, B, 0\}$, where B is the component of incident magnetic field $\mathbf{B}$.

iii. Velocity of fluid vary in the directions θ and r but is zero in z. Velocity is then: $\mathbf{u} = \{u_r, u_\theta, 0\}$, where u_r and u_θ are fluid velocities in r and θ directions respectively.

iv. Temperature of fluid vary in the directions θ and r but is zero in z. Temperature is then: $T = \{T_r,\, T_\theta,\, 0\}$, where T_r and T_θ are fluid temperatures in r and θ directions respectively.

v. The the square of electric current density is $\mathcal{J}^2 = (B\sigma)^2 (u_r - u_\theta)^2$, where σ is electrical conductivity.

2.2 Governing equations

They are written in cylindrical coordinates considering aforementioned assumptions. They are: The heat energy equation [4] is given by:

$$0 = \frac{1}{\rho c_p}\left[\frac{k}{r}\frac{\partial T}{\partial r} + k\frac{\partial^2 T}{\partial r^2} + \frac{k}{r^2}\frac{\partial^2 T}{\partial \theta^2} + B^2\sigma\left(u_r - u_\theta\right)^2\right] \tag{1}$$

Boundary conditions being: $\frac{\partial T}{\partial r} = \frac{\partial T}{\partial \theta} = 0$ and $T = T_0$ when $\mathcal{P} = 0$, $T = T_1$ when $\mathcal{P} = r$ on Γ. where c_p is specific heat capacity of the fluid, T thermodynamic temperature, k thermal conductivity of fluid, ρ is fluid density and $\mathcal{P}$ is length of r measured from ellipse's centre. Elliptical cross section of pipe [2] is given as $r^2 = \frac{a^2 b^2}{a^2 \sin^2\theta + b^2\cos^2\theta}$ as shown in figure 1,[7]. a and b are half of the ellipse's major and minor axes respectively. The equation of continuity is given by [9] :$\frac{1}{r}\frac{\partial}{\partial r}\left(ru_r\right) + \frac{1}{r}\frac{\partial}{\partial \theta}\left(u_\theta\right) = 0$ and Ohms law of electromagnetism is given by [5]: $\mathcal{J} = \sigma(\mathbf{E} + \mathbf{u} \times \mathbf{B})$, where $\mathbf{E}$ is electric field.

2.2.1 Non-dimensionalisation of heat energy equation

To non-dimensionalise heat energy equation (1), the following non-dimensional parameters are used [10]: $r = r^\star R, \theta = \theta^\star, u_r = u_r^\star U_0$, $u_\theta = u_\theta^\star U_0$, $T = T^\star(T_0 - T_1) + T_1$, Prandtl number, $Pr = \frac{\mu c_p}{k}$, Hartmann number, $Ha = BR\left(\frac{\sigma}{\mu}\right)^{\frac{1}{2}}$, Eckert number, $Ec = \frac{U_0^2}{c_p(T_0 - T_1)}$, where U_0 and R are a characteristic velocity and a characteristic length . Quantities with superscript star are dimensionless quantities. From equation (1), $\frac{\partial T}{\partial r} = \frac{\partial r^\star}{\partial r}\frac{\partial T}{\partial T^\star}\frac{\partial T^\star}{\partial r^\star} = \frac{(T_0 - T_1)}{R}\frac{\partial T^\star}{\partial r^\star}$, repeating the same process, expressions for other terms are worked out and set in (1), multiplied through by $\frac{\rho R^2}{\mu(T_0 - T_1)}$. Dimensionless numbers are put in the resulting equation and on neglecting $\star$'s, equation (1) becomes,

$$\frac{1}{Pr}\left[\frac{1}{r}\frac{\partial T}{\partial r} + \frac{\partial^2 T}{\partial r^2} + \frac{1}{r^2}\frac{\partial^2 T}{\partial \theta^2}\right] + EcHa^2(u_r - u_\theta)^2 = 0 \tag{2}$$

2.2.2 Heat energy equation in terms of stream function

Stream function, ψ, is introduced in equation (2). Given that $u_r = \frac{1}{r}\frac{\partial \psi}{\partial \theta}$ and $u_\theta = -\frac{\partial \psi}{\partial r}$ then

$$\frac{1}{Pr}\left[\frac{1}{r}\frac{\partial T}{\partial r} + \frac{\partial^2 T}{\partial r^2} + \frac{1}{r^2}\frac{\partial^2 T}{\partial \theta^2}\right] + EcHa^2\left(\frac{1}{r}\frac{\partial \psi}{\partial \theta} + \frac{\partial \psi}{\partial r}\right)^2 = 0 \tag{3}$$

Boundary conditions: $\frac{1}{r}\frac{\partial \psi}{\partial \theta} = -\frac{\partial \psi}{\partial r} = 0$, $\frac{\partial T}{\partial r} = \frac{\partial T}{\partial \theta} = 0$, $T = T_0$ when $\mathcal{P} = 0, T = T_1$ when $\mathcal{P} = r$ on Γ.

3 Numerical Solution of the Problem

3.1 Similarity Transformation

Equation (3) is converted into an ordinary differential equation using similarity transformation, Abbott *et.al* [6]. The similarity transformations used are of the form $\tau = \epsilon^\eta$ and $\eta = r^{-1}\theta^{-1}$ such that $T = h(\epsilon^{r^{-1}\theta^{-1}})$ and $\psi = f(\epsilon^{r^{-1}\theta^{-1}})$, where ϵ is the base of the natural logarithm. Then, $\frac{\partial T}{\partial r} = \frac{\partial}{\partial r}\left[h(\epsilon^{r^{-1}\theta^{-1}})\right] = -r^{-2}\theta^{-1}\epsilon^{r^{-1}\theta^{-1}}h'(\epsilon^{r^{-1}\theta^{-1}})$. The procedure is repeated for other terms in equation (3) with expressions obtained being inserted in equation (3). The resulting equation is multiplied through by r^2 and then only terms whose coefficients are $r^{-1}\theta^{-1}$ or their powers multiples are selected. Given that $\tau = \epsilon^{r^{-1}\theta^{-1}}$, equation (3) metamorphoses to

$$\frac{1}{Pr}\left[\tau log\tau h''(\tau) + h'(\tau) + log\tau h'(\tau)\right] + \tau log\tau EcHa^2\left[\left[f'(\tau)\right]^2\right] = 0 \tag{4}$$

Boundary conditions being: $f(\tau) = h(\tau) = 0$ and $f'(\tau) = h'(\tau) = 0$

3.2 Finite Element Method (FEM)

Equation (4) is solved using Finite Element Method (FEM) [11]. From equation (4), Ha, Pr and Ec are known, $h(\tau)$ is the scalar unknown. $f(\tau)$ is also known since it was worked out first when examining velocity profile [7]. Let the solution of $f(\tau)$ be g so that equation (4) becomes

$$\frac{1}{Pr}\left[\tau log\tau h''(\tau) + h'(\tau) + log\tau h'(\tau)\right] + \tau log\tau EcHa^2 g^2 = 0 \tag{5}$$

Boundary conditions lessen to: $h(\tau) = h'(\tau) = 0$. The FEM solution has E elements and $N = E + 1$ nodes. The approximate solution is C^0 continuous, i.e only the 0^{th} order solution is continuous across element interfaces.

3.2.1 Method of weighted residuals

The weak form of equation (5) is obtained using method of weighted residuals as follows: The residual of the differential equation is obtained by collecting all the terms on one side of the equation, the residual is minimized, second order derivative is lowered by integration by parts so that equation (5) gives

$$\int_{\Omega}\left(-\frac{1}{Pr}w'(\tau)\tau log\tau h'(\tau)+w(\tau)\tau log\tau EcHa^2g^2\right)d\tau$$

$$=-\frac{1}{Pr}\int_{\Gamma}w(\tau)\tau log\tau h'(\tau)n_{\tau}d\Gamma \tag{6}$$

where n_τ is the τ component of unit outward normal of the boundary. n_τ is equal to -1 and 1 at the left and right boundaries of the problem domain respectively.

3.2.2 Boundary conditions

The last term of equation (6) is the boundary integral, it provides the primary, $h = h_0$ and secondary variables, $\tau log\tau h'(\tau)n_\tau = p_0$ of the problem. For the Natural boundary condition, the secondary variable inside the boundary integral is simply replaced by the specified p_0 value as: $-\int_\Gamma w(\tau)\tau log\tau h'(\tau)n_\tau d\Gamma = -\int_\Gamma w(\tau)p_0 d\Gamma$

3.2.3 An approximate solution using shape functions and Galerkin method

If the desired C^0 continuous approximate solution is $h_{app}(\tau)=\sum_{j=1}^{N}h_j s_j(\tau)$, where h_{app} is the approximate solution to be found, N is the number of nodes in the finite element mesh, h_j's are the nodal unknown values that will be calculated at the end of finite element solution and s_j's are the shape (basis) functions that are used to construct the approximate solution. The shape functions have compact support and possess Kronecker-delta property. In Galerkin method, weight functions of equation (6) are chosen such that they are the same as those of shape function i.e $w(\tau) = s_i(\tau)$. Settling $h_{app}(\tau) = \sum_{j=1}^{N}h_j s_j(\tau)$ and $w(\tau) = s_i(\tau)$ in equation (6), produces

$$\sum_{j=1}^{N}\left[\int_{\Omega}\left(-\frac{1}{Pr}\tau log\tau s_i'(\tau)s_j'(\tau)\right)d\tau\right]h_j$$

$$=-\int_{\Omega}s_i(\tau)\tau log\tau EcHa^2g^2d\tau-\frac{1}{Pr}\int_{\Gamma}s_i(\tau)SVd\Gamma \qquad i=1,2,...,N \tag{7}$$

3.2.4 Global equation and elemental systems

Equation (7) is expressed in global equation system in matrix notation given by $[I]\{J\} = \{K\} + \{L\}$, where I is the square stiffness matrix of size $N \times N$, $\{J\}$ is is the vector of nodal unknowns with N entries. $\{K\}$ and $\{L\}$ are the global force vector and boundary integral vector respectively each of size $N \times 1$. From equation (7),

$$I_{ij} = \int_{\Omega} \left(-\frac{1}{Pr} \tau log\tau s_i'(\tau) s_j'(\tau) \right) d\tau,\ J_j = h_j,$$

$$K_i = -\int_{\Omega} s_i(\tau) \tau log\tau EcHa^2 g^2 d\tau \quad \text{and} \quad L_i = -\frac{1}{Pr} \int_{\Gamma} s_i(\eta) SV d\Gamma \tag{8}$$

$[I]$ is evaluated over the whole problem. Temperature is considered constant at boundary so that $\{L\}$ is also constant at boundaries. $\{K\}$ is considered varying over the whole domain since it depends on fluid velocity which is maximum at the centre of pipe but decreases towards periphery of pipe. Let $L_i = -\frac{1}{Pr} I_{21}^1$, where I_{21}^1 is defined in § 3.2.6 and let it be $I_{21} = \int_{\Gamma} s_i(\tau) SV d\Gamma$. The elemental stiffness matrix is given by

$$I_{ij}^e = \int_{\Omega} \left(-\frac{1}{Pr} \tau log\tau s_i'(\tau) s_j'(\tau) \right) d\tau \tag{9}$$

3.2.5 Gauss quadrature integration

To find I_{ij}^e integral using Gauss quadrature, limits of the integral are changed to be -1 and 1 which require change of variable. This leads to the use of master element in evaluating elemental integrals. Using the Kroncker-delta property of shape functions, they are written in terms of the master element coordinate ξ as

$$s_1 = \frac{1}{2}(1 - \xi) \text{ and } s_2 = \frac{1}{2}(1 + \xi) \tag{10}$$

To evaluate I_{ij}^e integrals, the global τ coordinate is related to ξ coordinate by

$$\tau = \frac{h^e}{2} \xi + \frac{\tau_1^e + \tau_2^e}{2} \tag{11}$$

where h^e is the length of element e given by $h^e = \tau_2^e - \tau_1^e$, τ_1^e and τ_2^e are the coordinates of the two end points of the element. Equation (9) is now written using the ξ coordinate and new limits for Gauss quadrature integration and transforms to

$$I_{ij}^e = \int_{-1}^{1} \left(-\frac{1}{Pr} \tau log\tau \frac{ds_i}{d\xi} \frac{ds_j}{d\xi} \frac{1}{J^e} \right) d\xi \tag{12}$$

where Finite Element Jacobian $= J^e = \frac{d\tau}{d\xi} = \frac{h^e}{2}$.

3.2.6 Assembly process

Elemental stiffness matrices are gathered in proper locations of the global system of equations. For instance, for a mesh of 6 linear elements with global node numbers, local to global node mapping matrix produces the following global equation system for 6 node mesh

$$\begin{bmatrix} I_{11}^1 & I_{12}^1 & 0 & 0 & 0 & 0 \\ I_{21}^1 & I_{22}^1 + I_{11}^2 & I_{12}^2 & 0 & 0 & 0 \\ 0 & I_{21}^2 & I_{22}^2 + I_{11}^3 & I_{12}^3 & 0 & 0 \\ 0 & 0 & I_{21}^3 & I_{22}^3 + I_{11}^4 & I_{12}^4 & 0 \\ 0 & 0 & 0 & I_{21}^4 & I_{22}^4 + I_{11}^5 & I_{12}^5 \\ 0 & 0 & 0 & 0 & I_{21}^5 & I_{22}^5 + I_{11}^6 \end{bmatrix} \begin{Bmatrix} h_1 \\ h_2 \\ h_3 \\ h_4 \\ h_5 \\ h_6 \end{Bmatrix}$$

$$= \begin{Bmatrix} K_1^1 \\ K_2^1 + K_1^2 \\ K_2^2 + K_1^3 \\ K_2^3 + K_1^4 \\ K_2^4 + K_1^5 \\ K_2^5 \end{Bmatrix} + \begin{Bmatrix} L_1^1 \\ L_2^1 + L_1^2 \\ L_2^2 + L_1^3 \\ L_2^3 + L_1^4 \\ L_2^4 + L_1^5 \\ L_2^5 \end{Bmatrix} \tag{13}$$

The boundary integral vector $\{L\}$ is evaluated at the boundary nodes of the problem domain. For the 6 node mesh, $L_1 = L_2 = L_3 = L_4 = L_5 = L_6 = -\frac{1}{Pr} I_{21}$ since temperature is constant at the boundary. L_i's are put in equation (13). From equation (8), the elemental force vector is given by $K_i = -\int_\Omega s_i(\tau) \tau log\tau EcHa^2 g^2 d\xi$. g which is fluid velocity will be a specific value at a specific node, g_i, Kweyu *et.al* [7]. The elemental force vector components are evaluated and placed in equation resulting from equation (13), which when trimmed delivers

$$\begin{bmatrix} I_{22}^1 + I_{11}^2 & I_{12}^2 & 0 & 0 \\ I_{21}^2 & I_{22}^2 + I_{11}^3 & I_{12}^3 & 0 \\ 0 & I_{21}^3 & I_{22}^3 + I_{11}^4 & I_{12}^4 \\ 0 & 0 & I_{21}^4 & I_{22}^4 + I_{11}^5 \end{bmatrix} \begin{Bmatrix} h_2 \\ h_3 \\ h_4 \\ h_5 \end{Bmatrix}$$

$$= \begin{Bmatrix} 0.00180344 EcHa^2 g_i^2 \\ 0.00180344 EcHa^2 g_i^2 \\ 0.00180344 EcHa^2 g_i^2 \\ 0.00180344 EcHa^2 g_i^2 \end{Bmatrix} - \begin{Bmatrix} \frac{1}{Pr} I_{21} \\ \vdots \\ \vdots \\ \vdots \end{Bmatrix} \tag{14}$$

3.2.7 Discretization of major axis of elliptical cross section of pipe

The major axis of the elliptical cross section of the pipe is sub divided into N elements and N+I nodes as shown in figure 2, [7].

3.2.8 Calculation of elemental stiffness matrix

Elemental stiffness matrix is found using equations (10), (11) and (12) such that: Settling $h^e = 0.0002, \tau_1^e = 0.0000$ and $\tau_2^e = 0.0002$ then $\tau = 0.0001\xi + 0.0001$ so that equation (12) grants

$$I_{ij}^e = \int_{-1}^{1} \left(-\frac{1}{Pr}(0.0001\xi + 0.0001) log(0.0001\xi + 0.0001) \frac{ds_i}{d\xi} \frac{ds_j}{d\xi} \frac{1}{J^e} \right) d\xi \quad (15)$$

Equation (15) is utilized to find components of the elemental stiffness matrix $I_{11}^e, I_{12}^e, I_{21}^e$ and I_{22}^e, outcomes are:

$$I_{11}^1 = \frac{0.00045086}{PrJ^e}, \quad I_{12}^1 = -\frac{0.00045086}{PrJ^e}, \quad I_{21}^1 = -\frac{0.00045086}{PrJ^e}, \quad I_{22}^1 = \frac{0.00045086}{PrJ^e} \quad (16)$$

The 2×2, $[I^e]$, elemental matrix, which comprises terms in equation (16), is given by

$$I^e = \begin{bmatrix} I_{11}^1 & I_{12}^1 \\ I_{21}^1 & I_{22}^1 \end{bmatrix} = \begin{bmatrix} \frac{0.00045086}{PrJ^e} & -\frac{0.00045086}{PrJ^e} \\ -\frac{0.00045086}{PrJ^e} & \frac{0.00045086}{PrJ^e} \end{bmatrix} \quad (17)$$

4 Results

The values of h for the first and last nodes of the discretized length of major axis are taken as $h_1 = h_{35} = 0.000$. This criterion will be implied in this section. Core velocity of the fluid is the velocity at the centre of the pipe, V_c. Velocity of fluid decreases from the centre of pipe towards the edges as shown in table 1 ,[7]. These values , f_i, will be adopted in finding h_i's in §4.1, §4.2 and §4.3. In particular, $V_c = f_{18}^1 = 1.895$.

4.1 Changing Prandtl number

Numerals for Prantl number varied are 0.5, 1.0 and 2.0, while $Ha = 1.0, J^e = 0.0001, Ec = 1.0, V_c = 1.895$ and $a = 0.0034$. When values of Pr and J^e are put in equation (17) an elemental matrix, I^e is formed. I^e is embraced to produce stiffness matrix I. Considering 35 nodes in figure 2 [7], substituting I, Ha, Ec, f_i and λ_θ in equation (14), a system of algebraic equations is formed. The equations are solved by utilizing Mathematica which provides solutions of h_j's as h_j^1's for $Pr = 0.5$, h_j^2's for $Pr = 1.0$ and h_j^3's for $Pr = 2.0$ in table 1 below. h_j's are the temperatures of fluid along the major axis of cross section of elliptical pipe.

Table 1: Temperatures along the major axis when $Pr = 0.5, 1.0, 2.0$

$h_1^1 = 0.000$ $h_1^2 = 0.000$ $h_1^3 = 0.000$	$h_2^1 = 33.01$ $h_2^2 = 16.52$ $h_2^3 = 8.286$	$h_3^1 = 64.02$ $h_3^2 = 32.04$ $h_3^3 = 16.08$	$h_4^1 = 93.03$ $h_4^2 = 46.56$ $h_4^3 = 23.36$	$h_5^1 = 120.0$ $h_5^2 = 60.08$ $h_5^3 = 30.15$	$h_6^1 = 145.0$ $h_6^2 = 72.59$ $h_6^3 = 36.43$	$h_7^1 = 168.0$ $h_7^2 = 84.11$ $h_7^3 = 42.21$
$h_8^1 = 189.1$ $h_8^2 = 94.62$ $h_8^3 = 47.49$	$h_9^1 = 208.1$ $h_9^2 = 104.1$ $h_9^3 = 52.66$	$h_{10}^1 = 225.1$ $h_{10}^2 = 112.6$ $h_{10}^3 = 56.54$	$h_{11}^1 = 240.1$ $h_{11}^2 = 136.7$ $h_{11}^3 = 60.31$	$h_{12}^1 = 253.1$ $h_{12}^2 = 126.7$ $h_{12}^3 = 63.58$	$h_{13}^1 = 264.1$ $h_{13}^2 = 132.2$ $h_{13}^3 = 66.34$	$h_{14}^1 = 273.1$ $h_{14}^2 = 136.7$ $h_{14}^3 = 68.61$
$h_{15}^1 = 280.1$ $h_{15}^2 = 140.2$ $h_{15}^3 = 70.37$	$h_{16}^1 = 285.1$ $h_{16}^2 = 142.7$ $h_{16}^3 = 71.62$	$h_{17}^1 = 288.1$ $h_{17}^2 = 144.2$ $h_{17}^3 = 72.38$	$h_{18}^1 = 289.1$ $h_{18}^2 = 144.7$ $h_{18}^3 = 72.63$	$h_{19}^1 = 288.1$ $h_{19}^2 = 144.2$ $h_{19}^3 = 72.38$	$h_{20}^1 = 285.1$ $h_{20}^2 = 142.7$ $h_{20}^3 = 71.62$	$h_{21}^1 = 280.1$ $h_{21}^2 = 140.2$ $h_{21}^3 = 70.37$
$h_{22}^1 = 273.1$ $h_{22}^2 = 136.7$ $h_{22}^3 = 68.61$	$h_{23}^1 = 264.1$ $h_{23}^2 = 132.2$ $h_{23}^3 = 66.35$	$h_{24}^1 = 253.1$ $h_{24}^2 = 126.7$ $h_{24}^3 = 63.58$	$h_{25}^1 = 240.1$ $h_{25}^2 = 120.2$ $h_{25}^3 = 60.31$	$h_{26}^1 = 225.1$ $h_{26}^2 = 112.6$ $h_{26}^3 = 56.55$	$h_{27}^1 = 208.1$ $h_{27}^2 = 104.1$ $h_{27}^3 = 52.27$	$h_{28}^1 = 189.1$ $h_{28}^2 = 94.62$ $h_{28}^3 = 47.50$
$h_{29}^1 = 168.1$ $h_{29}^2 = 84.11$ $h_{29}^3 = 42.22$	$h_{30}^1 = 145.0$ $h_{30}^2 = 72.60$ $h_{30}^3 = 36.44$	$h_{31}^1 = 120.0$ $h_{31}^2 = 60.08$ $h_{31}^3 = 30.16$	$h_{32}^1 = 93.03$ $h_{32}^2 = 46.56$ $h_{32}^3 = 23.37$	$h_{33}^1 = 64.02$ $h_{33}^2 = 32.04$ $h_{33}^3 = 16.08$	$h_{34}^1 = 33.01$ $h_{34}^2 = 16.52$ $h_{34}^3 = 8.292$	$h_{35}^1 = 0.000$ $h_{35}^2 = 0.000$ $h_{35}^3 = 0.000$

Fusing temperatures in table 1 above gives form in figure 1.

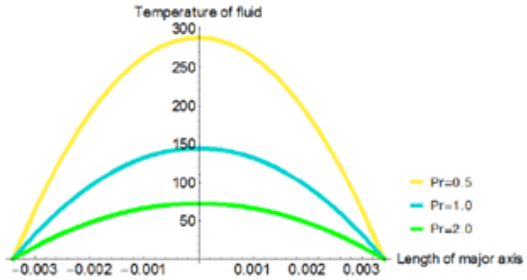

Figure 1: Combined temperature distributions for $Pr = 0.5$, $Pr = 1.0$ and $Pr = 2.0$

4.2 Diversifying Hartmann number

Hartmann number values employed are 5.0, 20.0 and 40.0 when $J^e = 0.0001$, $Pr = 1.0$, $Ec = 1.0$, $V_c = 1.895$ and $a = 0.0034$. Using the same method in §4.1 by applying above mentioned values, Mathematica supplies solutions in table 2.

Table 2: Temperatures along the major axis for $Ha = 5.0, 20.0, 40.0$

$h_1^1 = 0.000$ $h_1^2 = 0.000$ $h_1^3 = 0.000$	$h_2^1 = 17.03$ $h_2^2 = 24.91$ $h_2^3 = 50.15$	$h_3^1 = 33.05$ $h_3^2 = 48.70$ $h_3^3 = 98.91$	$h_4^1 = 48.05$ $h_4^2 = 71.20$ $h_4^3 = 145.3$	$h_5^1 = 62.02$ $h_5^2 = 92.30$ $h_5^3 = 189.2$	$h_6^1 = 74.97$ $h_6^2 = 111.9$ $h_6^3 = 230.2$	$h_7^1 = 86.88$ $h_7^2 = 130.0$ $h_7^3 = 268.1$
$h_8^1 = 97.76$ $h_8^2 = 146.6$ $h_8^3 = 302.8$	$h_9^1 = 107.6$ $h_9^2 = 161.6$ $h_9^3 = 334.2$	$h_{10}^1 = 116.4$ $h_{10}^2 = 175.0$ $h_{10}^3 = 362.4$	$h_{11}^1 = 124.2$ $h_{11}^2 = 186.8$ $h_{11}^3 = 387.3$	$h_{12}^1 = 130.9$ $h_{12}^2 = 197.1$ $h_{12}^3 = 409.0$	$h_{13}^1 = 136.6$ $h_{13}^2 = 205.8$ $h_{13}^3 = 428.0$	$h_{14}^1 = 141.3$ $h_{14}^2 = 213.0$ $h_{14}^3 = 442.3$
$h_{15}^1 = 144.9$ $h_{15}^2 = 218.5$ $h_{15}^3 = 454.1$	$h_{16}^1 = 147.5$ $h_{16}^2 = 222.5$ $h_{16}^3 = 462.5$	$h_{17}^1 = 149.1$ $h_{17}^2 = 224.9$ $h_{17}^3 = 467.7$	$h_{18}^1 = 149.6$ $h_{18}^2 = 225.6$ $h_{18}^3 = 469.6$	$h_{19}^1 = 149.1$ $h_{19}^2 = 225.0$ $h_{19}^3 = 468.1$	$h_{20}^1 = 147.5$ $h_{20}^2 = 222.7$ $h_{20}^3 = 463.4$	$h_{21}^1 = 144.9$ $h_{21}^2 = 218.8$ $h_{21}^3 = 455.3$
$h_{22}^1 = 141.3$ $h_{22}^2 = 213.4$ $h_{22}^3 = 444.0$	$h_{23}^1 = 136.7$ $h_{23}^2 = 206.3$ $h_{23}^3 = 429.4$	$h_{24}^1 = 131.0$ $h_{24}^2 = 197.7$ $h_{24}^3 = 411.4$	$h_{25}^1 = 124.2$ $h_{25}^2 = 187.6$ $h_{25}^3 = 390.2$	$h_{26}^1 = 116.5$ $h_{26}^2 = 175.8$ $h_{26}^3 = 365.7$	$h_{27}^1 = 107.7$ $h_{27}^2 = 162.5$ $h_{27}^3 = 337.9$	$h_{28}^1 = 97.82$ $h_{28}^2 = 147.6$ $h_{28}^3 = 306.8$
$h_{29}^1 = 86.95$ $h_{29}^2 = 131.1$ $h_{29}^3 = 272.3$	$h_{30}^1 = 75.04$ $h_{30}^2 = 113.0$ $h_{30}^3 = 234.6$	$h_{31}^1 = 62.09$ $h_{31}^2 = 93.41$ $h_{31}^3 = 193.7$	$h_{32}^1 = 48.11$ $h_{32}^2 = 72.24$ $h_{32}^3 = 149.5$	$h_{33}^1 = 33.10$ $h_{33}^2 = 49.56$ $h_{33}^3 = 102.2$	$h_{34}^1 = 17.06$ $h_{34}^2 = 25.39$ $h_{34}^3 = 52.06$	$h_{35}^1 = 0.000$ $h_{35}^2 = 0.000$ $h_{35}^3 = 0.000$

Blending temperatures in table 2 leads to outlines shown in figure 2.

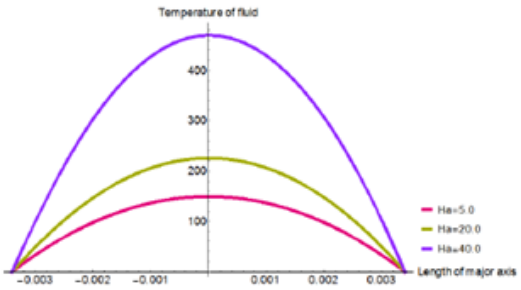

Figure 2: Fused temperature distributions for $Ha = 5.0$, $Ha = 20.0$ and $Ha = 40.0$

4.3 Altering Eckert number

Eckert number values varied are 5.0, 20.0 and 40.0 while $J^e = 0.0001, Pr = 1.0, Ha = 1.0, V_c = 1.895$ and $a = 0.0034$. Following the same steps as in §4.1 and engaging criterion above furnishes temperatures in table 3.

Table 3: Temperatures along the major axis with $Ec = 5.0, 20.0, 40.0$

$h_1^1 = 0.000$	$h_2^1 = 16.60$	$h_3^1 = 32.21$	$h_4^1 = 46.81$	$h_5^1 = 60.40$	$h_6^1 = 72.99$	$h_7^1 = 84.57$
$h_1^2 = 0.000$	$h_2^2 = 16.92$	$h_3^2 = 32.84$	$h_4^2 = 47.74$	$h_5^2 = 61.62$	$h_6^2 = 74.47$	$h_7^2 = 86.30$
$h_1^3 = 0.000$	$h_2^3 = 17.34$	$h_3^3 = 33.67$	$h_4^3 = 48.97$	$h_5^3 = 63.23$	$h_6^3 = 76.44$	$h_7^3 = 88.60$
$h_8^1 = 95.15$	$h_9^1 = 104.7$	$h_{10}^1 = 113.3$	$h_{11}^1 = 120.8$	$h_{12}^1 = 127.4$	$h_{13}^1 = 132.9$	$h_{14}^1 = 137.4$
$h_8^2 = 97.11$	$h_9^2 = 106.9$	$h_{10}^2 = 115.6$	$h_{11}^2 = 123.3$	$h_{12}^2 = 130.0$	$h_{13}^2 = 135.7$	$h_{14}^2 = 140.3$
$h_8^3 = 99.71$	$h_9^3 = 109.8$	$h_{10}^3 = 118.7$	$h_{11}^3 = 126.7$	$h_{12}^3 = 133.6$	$h_{13}^3 = 139.4$	$h_{14}^3 = 144.1$
$h_{15}^1 = 141.0$	$h_{16}^1 = 143.5$	$h_{17}^1 = 145.0$	$h_{18}^1 = 145.5$	$h_{19}^1 = 145.0$	$h_{20}^1 = 143.5$	$h_{21}^1 = 141.0$
$h_{15}^2 = 143.9$	$h_{16}^2 = 146.5$	$h_{17}^2 = 148.1$	$h_{18}^2 = 148.6$	$h_{19}^2 = 148.1$	$h_{20}^2 = 146.5$	$h_{21}^2 = 143.9$
$h_{15}^3 = 147.9$	$h_{16}^3 = 150.5$	$h_{17}^3 = 152.1$	$h_{18}^3 = 152.6$	$h_{19}^3 = 152.1$	$h_{20}^3 = 150.5$	$h_{21}^3 = 147.9$
$h_{22}^1 = 137.5$	$h_{23}^1 = 132.9$	$h_{24}^1 = 127.4$	$h_{25}^1 = 120.8$	$h_{26}^1 = 113.3$	$h_{27}^1 = 104.7$	$h_{28}^1 = 95.16$
$h_{22}^2 = 140.3$	$h_{23}^2 = 135.7$	$h_{24}^2 = 130.1$	$h_{25}^2 = 123.4$	$h_{26}^2 = 115.7$	$h_{27}^2 = 106.9$	$h_{28}^2 = 97.16$
$h_{22}^3 = 144.2$	$h_{23}^3 = 139.4$	$h_{24}^3 = 133.6$	$h_{25}^3 = 126.8$	$h_{26}^3 = 118.8$	$h_{27}^3 = 109.8$	$h_{28}^3 = 99.81$
$h_{29}^1 = 84.58$	$h_{30}^1 = 73.00$	$h_{31}^1 = 60.41$	$h_{32}^1 = 46.82$	$h_{33}^1 = 32.22$	$h_{34}^1 = 16.61$	$h_{35}^1 = 0.000$
$h_{29}^2 = 86.36$	$h_{30}^2 = 74.53$	$h_{31}^2 = 61.67$	$h_{32}^2 = 47.79$	$h_{33}^2 = 32.88$	$h_{34}^2 = 16.95$	$h_{35}^2 = 0.000$
$h_{29}^3 = 88.71$	$h_{30}^3 = 76.55$	$h_{31}^3 = 63.34$	$h_{32}^3 = 49.07$	$h_{33}^3 = 33.75$	$h_{34}^3 = 17.39$	$h_{35}^3 = 0.000$

Incorporating temperatures in table 3, presents profiles in figure 3.

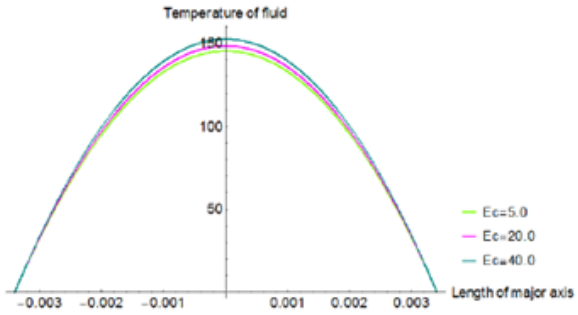

Figure 3: Mixed temperature profiles for $Ec = 5.0, Ec = 20.0$ and $Ec = 40.0$

5 Conclusion

Temperature outlines for MHD flow in a straight horizontal pipe of elliptical cross section has been described. Solutions are represented in terms of tables and graphs and divulge that: When Prantl number is increased, peak temperature decreases, figure 1. Peak temperature increases when Hartmann and Eckert numbers are increased (figures 2 and 3), peak temperature being more pronounced for Hartmann number. In all the three scenarios, temperature decreases towards the edges of the pipe.

References

[1] A. Abdulhassan, M. Ammar and S. Nabeel, Numerical Study of Heat Transfer and Flow of Nanofluid Using Multi-Phase Mixture Model through Elliptical Tubes, *Journal of University of Babylon for Engineering Sciences*, **26** (2018), 294-308.

[2] A. Adrian, *Solid Analytic Geometry*, Dover Publications, Dover, 2016.

[3] A. Malekzade, H. Amir and M. Jahangiri, Magnetic Field Effect on Laminar Heat Transfer in a Pipe for Entry Region, *Journal of Mechanical Science and Technology*, **25** (2011), 877-884. https://doi.org/10.1007/s12206-011-0140-6

[4] A. Morrison, *An Introduction to Fluid Mechanics*, Cambridge University Press, Cambridge, 2013.

[5] A. Zangwill, *Modern Electrodynamics*, Cambridge University Press, Cambridge, 2013.

[6] D. Abbott, H. Arthur and Tsung-Yen, *Similarity Analyses of Partial Differential Equations*, ORA project, The University of Michigan, (1967), 1-130.

[7] D. Kweyu, J. Bitok and W. Manyonge, Velocity Profile for Magnetohydrodynamic flow in straight Horizontal Elliptical Pipe,*Applied Mathematical Sciences*, **15** (2021), 283-295. https://doi.org/10.12988/ams.2021.914486

[8] E. Gedik, H. Kurt and Z. Zecebli, CFD Simulation of Magnetohydrodynamic Flow of a Liquid-Metal Galistan Fluid in Circular Pipes, *FDMP*, **9** (2013), 23-33.

[9] J. Alexander, *A Physical Introduction to Fluid Dynamics*, John Wiley, New York, 2014.

[10] K. Josef, *Dimensionless Physical Quantities in Science and Engineering*, Elsevier, London, 2012. https://doi.org/10.1016/c2011-0-06212-9

[11] S. Rao, *The Finite Element Method in Engineering*, Elsevier, Oxford, 2018.

Received: May 9, 2021; Published: June 11, 2021